Progress on Quantitative Modeling of rf Sheaths

D. A. D'Ippolito, J. R. Myra, H. Kohno and J. C. Wright

Lodestar Research Corporation,
Boulder, Colorado, 80301

May, 2011

Prepared for the 19th Topical Conference on Radio Frequency Power in Plasmas, Newport, Rhode Island, June 1 – 3, 2011.

DOE/ER/54392-65 & ER/54823-12 LRC-11-143

Lodestar Research Corporation

2400 Central Avenue #P-5

Boulder, CO 80301

Progress on Quantitative Modeling of rf Sheaths

D. A. D'Ippolito[a], J. R. Myra[a], H. Kohno[b], and J. C. Wright[b]

[a]*Lodestar Research Corporation, 2400 Central Avenue, #P-5, Boulder, Colorado, 80301USA*
[b]*Plasma Science and Fusion Center, MIT, Cambridge, Massachusetts, 02139USA*

Abstract. A new quantitative approach for computing the rf sheath potential is described, which incorporates plasma dielectric effects and the relative geometry of the magnetic field and the material boundaries. The new approach uses a modified boundary condition ("rf sheath BC") that couples the rf waves and the sheaths at the boundary. It treats the sheath as a thin vacuum region and matches the fields across the plasma-vacuum boundary. When combined with the Child-Langmuir Law (relating the sheath width and sheath potential), the model permits a self-consistent determination of the sheath parameters and the rf electric field at the sheath-plasma boundary. Semi-analytic models using this BC predict a number of general features, including a sheath voltage threshold, a dimensionless parameter characterizing rf sheath effects, and the existence of sheath plasma waves with an associated resonance. Since the sheath BC is nonlinear and dependent on geometry, computing the sheath potential numerically is a challenging computational problem. Numerical results will be presented from a new parallel-processing finite-element rf wave code for the tokamak scrape-off layer (called "rfSOL"). The code has verified the physics predicted by analytic theory in 1D, and extended the solutions into model 2D geometries. The numerical calculations confirm the existence of multiple roots and hysteresis effects, and parameter studies have been carried out. Areas for future work will be discussed.

Keywords: rf sheath, ICRF, boundary condition, fast wave, slow wave
PACS: 52.35.Mw**,** 52.40.Kh, 52.50.Qt, 52.55.Fa

INTRODUCTION

Plasma heating and current drive with ion cyclotron range of frequency (ICRF) antennas has been quite successful in past tokamak experiments and is expected to play an important role in ITER. An important issue that must first be addressed is that of developing a *quantitative predictive capability for rf-enhanced sheaths* on the antenna, limiters and other boundary surfaces, which is needed for the design and interpretation of future experiments. Sheath-related issues include rf-specific impurity generation by enhanced sputtering and self-sputtering of material surfaces in contact with the rf waves, and power dissipation in the scrape-off-layer (SOL), leading to local hot spots and reduced power coupled to the core plasma. These parasitic effects impact (a) the functioning and survivability of the antennas, walls and divertors; (b) the choice of wall material and the lifetime of the boundary surfaces; (c) the heating efficiency of the ICRF antennas; and (d) the impurity concentration of edge and core

plasmas. Reviews of nonlinear ICRF interactions and an extensive list of references are given in Refs. 1 and 2. The requirements for control of radiofrequency (rf) sheaths are even more stringent in long-pulse or steady-state experiments than in present devices, which motivates a renewed interest in their study.

Sheath formation is a general phenomenon, associated with parasitic rf wave coupling. ICRF antennas are designed to launch a fast wave (FW), which propagates into the core plasma and is fully absorbed under conditions of high single pass damping. In practice, this is not always achieved: (i) the fast wave can propagate around the scrape-off-layer (SOL) and be partially absorbed by boundary structures; (ii) the single pass absorption in the core plasma can be low for some wave components, so that rf wave energy propagates through the plasma to the wall ("far field sheath"); and (iii) the FW antenna can also launch a slow wave (SW) component (either evanescent or propagating) in the SOL when the magnetic field is not perfectly aligned with the antenna structure, i.e. when the antenna current has a component parallel to the equilibrium magnetic field **B** (e.g. "near field" or "antenna" sheath). For mechanisms (i) and (ii), when the FW encounters a material structure, the Maxwell equation boundary conditions require that it couple to the SW at the wall.

In all these situations, the rf sheath forms when a SW comes in contact with a material boundary (wall, antenna or divertor). The strength of the sheath potential depends both on the wave polarization and on the equilibrium **B** field geometry. The SW component $E_{\|} = \mathbf{B}\cdot\mathbf{E}_{rf}/B$ accelerates electrons out of the plasma, with the result that a large (up to several hundred volts) rf sheath potential forms to confine the electrons and maintain ambipolarity. The plasma acts to rectify the oscillating rf voltage V_{rf} [see Fig. 1 in Ref. 1], producing a dc ("rectified") potential of order $e\Phi_0 \sim eV_{rf} + 3T_e$,[3,4] where $2V_{rf}$ is the difference between the highest and lowest values of the oscillating rf potential and $e\Phi_B \sim 3T_e$ is the usual Bohm result for thermal sheaths.

Until recently, a simple estimate of the driving voltage was used for sheath modeling, i.e.

$$V_{sh} = \int ds\, E_{\|} \quad , \tag{1}$$

where the integral is taken along the field line between contact points (for antenna sheaths) and is not well defined for cases where the two contact points are far apart unless $E_{\|}$ is localized near the surface by plasma effects. However, since most antenna codes require a vacuum region surrounding the metal structure, plasma effects are usually not included in evaluating Eq. (1). Finally, we note that in this approach V_{sh} is evaluated as a post-processing step after the rf fields are calculated, so there is no self-consistency between the rf fields and the sheath properties.

The subject of this paper is a new approach[5,6] to calculating the rf sheath potential that eliminates all of these difficulties. This approach is motivated by the following ordering

$$\lambda_D << \delta_e \sim L_{\|}(m_e/m_i)^{1/2} << \delta_i \quad , \tag{2}$$

showing that there is a scale separation between three characteristic lengths: the sheath width (~ Debye length λ_D), the perpendicular scale of the SW ($\sim \delta_e = c/\omega_{pe}$), and that of the FW ($\sim \delta_i = c/\omega_{pi}$). The first inequality in Eq. (2) suggests replacing the usual metallic wall boundary condition (BC) by a new "rf sheath BC" that incorporates the effect of the sheath directly into the solution for the rf fields. This approach allows incorporation of plasma dielectric and sheath capacitance effects, allows accurate representation of the magnetic field and wall geometry, and gives a local result for the sheath potential (useful for computing the surface distribution of the sheath voltage and for treating the far field sheath problem).

THE MODEL

To derive the sheath BC, the electron-poor sheath is treated as a thin vacuum region of width Δ with capacitance $\propto 1/\Delta$. The form of the BC is derived from the Maxwell equations using continuity of E_t and D_n across the vacuum-plasma interface,[5,6] which gives

$$\mathbf{E}_t = \nabla_t(\Delta D_n) \quad . \tag{3}$$

Here the rf fields are defined on the plasma side of the sheath-plasma interface with $\mathbf{D} = \varepsilon \cdot \mathbf{E}$, the subscripts n and t denote the directions normal and tangential to this interface (i.e. to the bounding surface), and the scalar dielectric constant in the vacuum sheath region is $\varepsilon_{sh} = 1$. Note that the usual metal wall BC ($\mathbf{E}_t = 0$) is recovered when the sheath term on the rhs is small.

This approach incorporates plasma effects through the dielectric tensor ε (dominated by the electron term with $\varepsilon_{||}$). The BC also depends on the detailed geometry of the **B** field relative to the boundary, as can be seen by estimating $D_n \approx \mathbf{n}\cdot\mathbf{b}\ \varepsilon_{||} E_{||}$, where **b** is the unit vector parallel to **B**, and **n** is the unit vector normal to the sheath. Using this result, and taking the electrostatic (ES) limit, we derive a dimensionless sheath capacitance parameter as follows: Eq. (3) implies that $-\Phi \sim \Delta(\mathbf{n}\cdot\mathbf{b}\ \varepsilon_{||} E_{||}) \equiv \mathbf{n}\cdot\mathbf{b}\ \Lambda\ \Phi$ where

$$\Lambda \equiv -ik_{||}\,\Delta\,\varepsilon_{||} \quad . \tag{4}$$

For the simplest case with the magnetic field normal to the boundary ($\mathbf{n}\cdot\mathbf{b} = 1$), there are three limits. When $|\Lambda| << 1$, the *conducting wall* limit of the BC is recovered ($\mathbf{E}_t = 0$), whereas $|\Lambda| >> 1$ gives the *insulating wall* limit ($D_n = 0$). For $\Lambda = 1$ there is the possibility of a *sheath-plasma-wave (SPW) resonance* when the SW is evanescent (see below). This is a series resonance, where the impedance of the capacitive current across the sheath balances that of the inductive plasma current into the sheath.

The complete sheath model combines Eq. (3) with three other relations. First, the sheath width Δ can be treated as constant (resulting in a linear problem) or it can be approximated by the dc sheath width satisfying the Child-Langmuir (CL) Law (giving a nonlinear problem). The CL constraint and the accompanying definitions are given by

$$\Delta = \lambda_D \left(e\Phi_0 / T_e \right)^{3/4} \quad , \tag{5}$$

$$\Phi_0 = C_{sh} V_{sh} + 3T_e / e \quad , \quad V_{sh} = \Delta \, | D_n | \quad . \tag{6}$$

As discussed above, V_{sh} is the amplitude of the oscillating voltage driving the sheath formation, obtained here by integrating across the thin ES sheath layer, Φ_0 is the dc rectified sheath potential, C_{sh} is an order unity rectification coefficient[3,4] and we have included the thermal (Bohm) sheath term as the low voltage limit. The full sheath model is given by Eqs. (3), (5) and (6); it determines the rf sheath potential, sheath width, and local rf field (D_n or $E_{||}$) self-consistently.

SEMI-ANALYTIC SOLUTIONS

The model just described has been applied to a number of analytic or semi-analytic calculations to explore the physics of the BC.[7-10] These include models of FW antenna sheaths,[7] wall sheaths[8,9] arising from SWs launched by the antenna, and far field sheaths[10] resulting from low single pass propagation of FWs across the core plasma. Here, we will summarize the results of three calculations which can be compared with the numerical solutions discussed in the next section.

When the **B** field is tilted with respect to the antenna (such that $\mathbf{b} \cdot \mathbf{J}_{ant} \neq 0$), the FW antenna launches an unwanted SW. A sketch of the situation and of the domain of our model problem is given in Fig. 1.

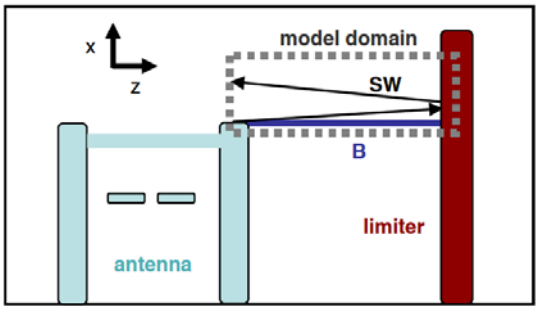

FIGURE 1. Schematic of SW propagation from antenna to limiters, looking down on the torus. Also shown is the domain of the model problems solved in Refs. 8 and 9. Reprinted from Ref. 9 with permission from the Institute of Physics.

At low density ($n_e < n_{LH} \equiv$ lower hybrid density), the electrostatic SW propagates along the magnetic field as a resonance cone (RC).[8] When it encounters a boundary, the RC reflects off the sheath, and the resulting sheath voltage depends on the parameter $\Lambda_0 = \Delta\varepsilon_{||} / a_{||} \sim P_{rf}^{3/8} n_e^{1/2}$, where $a_{||}$ is the width of the SW pulse of voltage V_0 launched at the antenna. In Ref. 8 it was shown that the fraction of the launched voltage transmitted to the sheath, V_{sh} / V_0 , becomes order unity above a threshold, $\Lambda_0 > 3$. The existence of the voltage threshold is a consequence of the nonlinear CL constraint for the self-consistent sheath width. For C-Mod parameters it is possible to satisfy the voltage threshold condition, so this mechanism may explain the observed rf interaction with the vessel surface.[11]

At high density ($n_e > n_{LH}$), the SW propagates along **B** (≈ along z) but is evanescent in the radial direction (x). If the limiter is far away, there is no coupling of the antenna to the limiter sheath. But the linear calculations in Ref. 9 (for specified sheath width) show that this coupling occurs when $L_{||} < \delta_i$ (sufficiently close limiters) and $\Lambda \equiv \Delta\varepsilon_{||} / L_{||} > 1$ (sufficiently strong driving voltage), where $L_{||}$ is the connection

length of the antenna to the limiter along the magnetic field. If these conditions are satisfied, the evanescent SW couples to the sheath plasma wave[10-13] (SPW), which propagates radially along the sheath boundary, carrying the rf voltage away from the antenna. Figure 2 shows an example of a SPW solution; in this case the parameters were chosen to localize the mode near the sheaths.

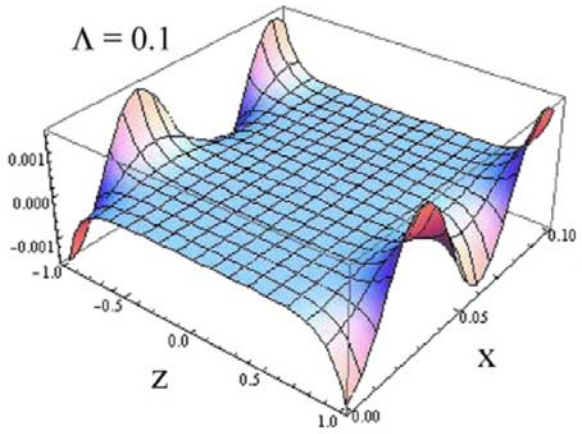

FIGURE 2. Spatial structure of Re $E_Z(x,z)$ for the SPW for the case $\Lambda = 0.1$. Reprinted from Ref. 9 with permission from the Institute of Physics

When the CL constraint is enforced (nonlinear solution), one finds that there are multiple roots with a characteristic hysteresis structure. We return to this point in the next section. In each case, the root represents a coupling of the evanescent SW to the SPW, which allows the voltage to propagate away from the antenna.

The previous two examples discussed slow waves which are launched at the antenna and drive sheaths in the vicinity of the antenna (e.g. on nearby limiters). As a third example, we discuss the case of far field sheaths,[6,10] which arise when the FW propagates away from the antenna and encounters a metallic boundary, e.g. in the case of low single pass absorption or propagation around the SOL. If the **B** field has a component normal to the wall (i.e. the wall is not a flux surface), the FW cannot satisfy the BC at the wall without coupling to the SW. (This is true even for the metal wall BC, but the sheath BC adds the possibility of multiple, higher voltage roots for the sheath potential.) A three-wave coupling analysis in Ref. 10 derived an expression for the FW-SW coupling from the sheath BC, viz.

$$E_{SW} = E_{FW} \frac{\mathbf{n}\cdot\mathbf{g}_0\times\mathbf{g}_1}{\mathbf{n}\cdot\mathbf{g}_1\times\mathbf{g}_2} \quad , \qquad \mathbf{g}_j = \mathbf{e}_j - i\Delta(\mathbf{n}\cdot\boldsymbol{\varepsilon}\cdot\mathbf{e}_j) \quad . \tag{6}$$

Here, j = 0, 1 and 2 denotes the incident and reflected FW and the coupled SW, respectively; $\mathbf{e}_j$ is the polarization unit vector for the constant density wave solution, and $\mathbf{g}_j$ is the generalization to include the sheath capacitance effect in the sheath BC. A numerical 1D solution of Eqs. (3), (5) and (6) showed that the self-consistent sheath BC permits multiple roots and the SPW resonance. The latter can occur if $\mathbf{g}_2 = 0$ (ES limit) or $\mathbf{g}_1\times\mathbf{g}_2 = 0$ (EM case). These results will be discussed in connection with the numerical solution in the next section.

NUMERICAL SOLUTIONS (RFSOL CODE)

We have shown that the sheath potential is sensitive to both the magnetic field and wall geometry. Thus, numerical methods are required to treat sheaths in realistic tokamak SOL geometry. The sheath BC approach allows a wave code to compute both the rf fields and the sheath quantities self-consistently, although the latter requires a nonlinear solver. In the past two years, a new code, rfSOL, was developed to treat rf waves and sheaths in the SOL.[14,15] This code uses finite element techniques to handle the geometry of the boundary and was parallelized to allow sufficient resolution for slow wave studies. Comparing the code solution with the analytic work, we find that rfSOL recovers the physics in the analytic models, but allows generalizations to include 2D geometry, density profiles, model antennas, spatially varying B fields, etc.

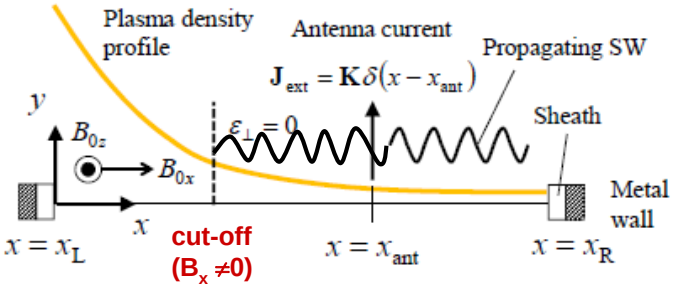

FIGURE 3. Schematic of a 1D model problem with a propagating SW trapped between the SW cut-off and the sheath.

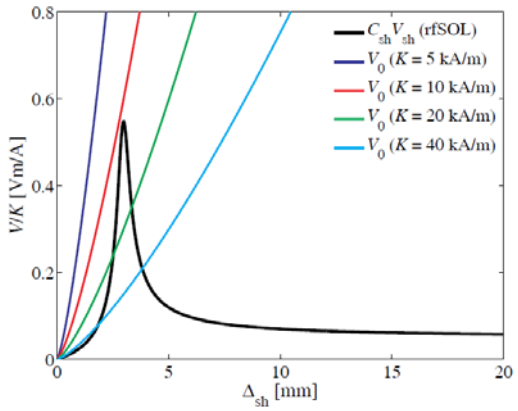

FIGURE 4. Graphical solution of the nonlinear sheath problem for different values of the antenna current K.

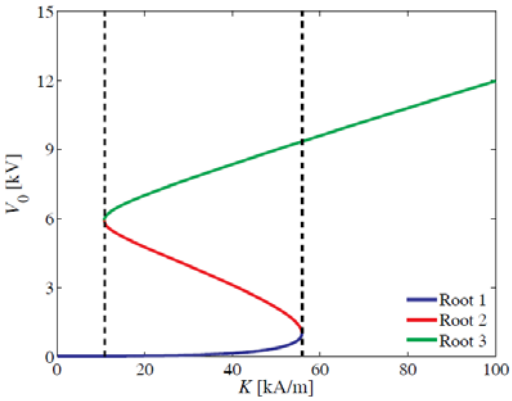

FIGURE 5. Root structure for the sheath potential with hysteresis curve, obtained from the nonlinear rfSOL solution.

As a first example, we discuss the case of a propagating SW in 1D with a constant **B** field tilted into the wall ($B_x \neq 0$). This tilt drives an rf sheath. As shown in Fig. 3, the antenna launches a SW that propagates up the density profile until a reflection point occurs where $\varepsilon_\perp = 0$; this reflection (instead of the usual lower-hybrid resonance) is due to $B_x \neq 0$, which changes the dispersion relation. A graphical solution of the self-consistent sheath problem is shown in Fig. 4, where the black line

denotes the rfSOL code solution for the rectified sheath potential $V_0 = C_{sh} V_{sh}$ (normalized to the antenna current K) for a specified value of sheath width Δ, and the colored curves give the function $V_0(\Delta)$ from the CL constraint, plotted vs. Δ. The peak in the black curve is due to a standing wave resonance, and finite dissipation was used to limit the height of the peak. Note that there are multiple roots for this nonlinear problem. In Fig. 5, the root structure is further illustrated by plotting the rfSOL solution for V_0 vs. the antenna current K. Note the hysteresis structure and the region of multiple roots. This type of structure was also observed in recent semi-analytic models[9,10] of sheaths in different physical regimes, and seems to be a general result. Note that this structure requires the sheath capacitance effect in the sheath BC together with the CL constraint enforcing self-consistency between the sheath width and sheath potential.

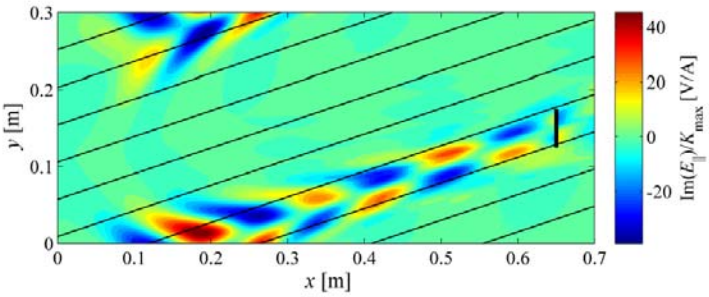

FIGURE 6. The 2D rfSOL solution for $Im(E_{||})/K$ of the SW with tilted B field in the *low density* limit. Here the rf wave and self-consistent sheath are computed, showing resonance cone propagation in both directions from the antenna.

Now we turn to 2D solutions with the rfSOL code. First, we consider the low-density case ($n_e < n_{LH}$) with constant **B** field tilted into the wall ($B_x \neq 0$). As predicted by simpler models,[8] the SW propagates as a resonance cone (see Fig. 6). The code solves for the self-consistent CL sheath at the right-hand boundary, and one finds that the sheath affects the phase shift of the wave reflected off the wall, which could affect the near field of the antenna. Comparing the solution for different values of the antenna current K, we find that $(D_n / K) \to 0$ as $K \to \infty$. This confirms the scaling $\Delta(D_n / K) \approx \text{const.}$, which follows from the sheath BC and illustrates the transition from the conducting ($\Delta \to 0$) to the insulating ($\Delta \to \infty$) limit as K (and hence Δ) increases.

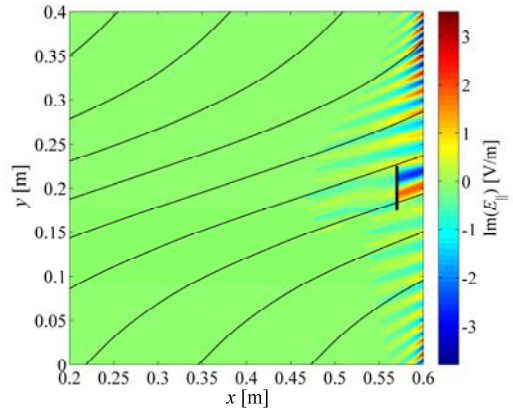

FIGURE 7. The 2D rfSOL solution for $Im(E_{||})$ of the SW with *curved **B** field* in the *high density* limit. The rf wave and self-consistent sheath are computed, showing an evanescent SW coupling to the sheath plasma wave (SPW). The poloidal asymmetry is due to the tilted and curved B field.

We have also investigated the 2D high-density case ($n_e > n_{LH}$) both for a constant tilted **B** field and for a model 2D curved **B** field. In this high-density limit, the SW launched by the antenna is evanescent but couples to the SPW, which propagates along the sheath, in agreement with earlier work.[9] The wave phase follows the field lines and couples k_x and k_y, which results in the observed poloidal asymmetry (Fig. 7).

SUMMARY AND FUTURE WORK

By a series of increasingly numerical calculations, we have demonstrated the tractability and physics content of the rf sheath BC. We have demonstrated SW sheath formation, sheath plasma waves, multiple roots, and obtained parametric dependences in simple geometries. In the future, the rfSOL code will be used to study more complicated geometries, leading eventually to a treatment of the tokamak SOL.

ACKNOWLEDGMENTS

We thank Paul Bonoli and the rf SciDAC team for many useful discussions. This work was supported by USDOE grants DE-FG02-97ER54392 and DE-FC02-05ER54823.

REFERENCES

1. J. R. Myra, D. A. D'Ippolito, D. A. Russell, L. A. Berry, E. F. Jaeger, and M. D. Carter, Nucl. Fusion **46**, S455 (2006).
2. J.-M. Noterdaeme and G. Van Oost, Plasma Phys. Control. Fusion **35**, 1481 (1993).
3. M. A. Lieberman, IEEE Trans. Plasma Sci. **16**, 638 (1988); V.A. Godyak and N. Sternberg, Phys. Rev. A **42**, 2299 (1990).
4. J. R. Myra, D. A. D'Ippolito and M. J. Gerver, Nucl. Fusion **30**, 845 (1990).
5. D. A. D'Ippolito and J. R. Myra, Phys. Plasmas **13**, 102508 (2006).
6 J. R. Myra, D. A. D'Ippolito, and M. Bures, Phys. Plasmas **1**, 2890 (1994).
7. D. A. D'Ippolito and J. R. Myra, Phys. Plasmas **16**, 022506 (2009); D. A. D'Ippolito and J. R. Myra, Phys. Plasmas **17**, 072508 (2010).
8. J. R. Myra and D. A. D'Ippolito, Phys. Rev. Lett. **101**, 195004 (2008).
9. J.R. Myra and D.A. D'Ippolito, Plasma Phys. Controlled Fusion **52**, 015003 (2010).
10. D. A. D'Ippolito, J. R. Myra, E. F. Jaeger, and L. A. Berry, Phys. Plasmas **15**, 102501 (2008).
11. S.J. Wukitch, et al., 21st IAEA Fusion Energy Conf., Chengdu, China, paper IAEA-CN-149-FT/1-6, (2006).
12. J. R. Myra, D. A. D'Ippolito, D. W. Forslund and J. U. Brackbill, Phys. Rev. Lett. **66**, 1173 (1991) and refs. therein.
13. R. L. Stenzel, Phys. Rev. Lett. **60**, 704 (1988) and Phys Fluids **B 1**, 2273 (1989); and references therein.
14. Haruhiko Kohno, J. R. Myra and D. A. D'Ippolito, presented at the *52nd Annual Meeting of the Division of Plasma Physics*, Chicago, Illinois, November 8 - 12, 2010, paper JP9-92.
15. Haruhiko Kohno, PhD thesis, MIT (2011).